Tandem Cu/ZnO/ZrO_2-SAPO-34 System for Dimethyl Ether (DME) Synthesis from CO_2 and H_2: Catalyst Optimization, Techno-Economic and Carbon-Footprint Analyses

Jasan Robey Mangalindan[1], Fatima Mahnaz[1], Jenna Vito[1], Navaporn Suphavilai[1], & Manish Shetty[1,]*

[1]Artie McFerrin Department of Chemical Engineering, 100 Spence Street, Texas A&M University, College Station, TX 77843, USA.

*Email. manish.shetty@tamu.edu

KEYWORDS. CO_2 utilization, sustainable fuels, C-C coupling, zeolite, SAPO-34, methanol, hydrogen storage.

ABSTRACT

To alleviate detrimental effects associated with anthropogenic emissions, the use of CO_2 and H_2 as feedstocks for their conversion to associated with dimethyl ether (DME) with tandem catalysts is an attractive and sustainable route. First, we investigated, for the first time, the catalytic activity of bifunctional admixtures of Cu-ZnO-ZrO_2 (CZZ) and a silicoaluminophosphate, SAPO-34, for CO_2 hydrogenation to DME, and optimized their reactivity with an emphasis on identifying optimum synthesis conditions for CZZ including Cu:Zn:Zr molar ratio, and ageing and calcination temperatures. The highest methanol (MeOH) productivity (10.8 mol kg_{cat}^{-1} h^{-1}) was observed for CZZ-611 aged at 40°C and calcined at 500°C. When coupled with SAPO-34, CZZ/SAPO-34 reached 20% CO_2 conversion and 56% DME selectivity at optimized conditions (260°C, 500 psig, and 2000 mL g_{CZZ}^{-1} h^{-1}) and was stable for 50 h time-on-stream. Next, we performed kinetic modeling to translate lab-scale findings to industrial packed-bed reactors followed by a techno-economic analysis (TEA) with cradle-to-gate environmental footprint evaluation to evaluate its industrial applicability. TEA of a 20,000 tpy DME plant revealed raw material costs as the main operating costs drivers (H_2 cost comprises 47% of total cost). Considering green H_2 ($4/kg H_2) and captured CO_2 as feed, the minimum DME selling price (MDSP) was $3.21/kg, ~3.6x higher than market price ($0.88/kg). MDSP drops to $1.99/kg with grey H_2 ($1/kg H_2) and fluctuates ±$0.14 with changes in CAPEX (±30%) and other economic factors. The plant's carbon footprint was mainly affected by H_2 source. Green and grey H_2 resulted in emissions of 0.21 and 4.4 kg CO_2 eq/kg DME, respectively. Importantly, negative carbon-footprint can be achieved by using green H_2 and CO_2 captured directly from air. Overall, our work showed tandem catalysis as a promising approach towards sustainable DME production and identifies the pathway towards making it cost-competitive with fossil-fuels.

INTRODUCTION

Anthropogenic carbon dioxide (CO_2) emissions have negatively impacted our environment resulting in rapid climate change caused by the increase in global surface temperatures.[1] Efforts to mitigate the effects of these emissions include the capture of CO_2 from point sources such as, industrial emissions or directly from the air, to prevent any further rise in atmospheric CO_2 levels.[2, 3] The captured CO_2 can be stored or utilized directly in chemical processes as a feedstock. Recently, interest has been drawn to the latter option, broadly classified as carbon dioxide utilization (CDU) techniques.[4, 5] Among many CDU techniques, the conversion of CO_2 as a feedstock to produce chemicals and fuels including methane, light olefins, paraffins, and alcohols, provides a potentially cleaner production route, compared to the fossil-based sources.[6-9] Specifically, the conversion of CO_2 to dimethyl ether (DME) is attractive, as DME can be utilized as a clean alternative to fossil fuels and used as a hydrogen (H_2) carrier.[4, 10, 11] Its non-toxic and non-carcinogenic properties together with its high-cetane number, good flammability, and ability to combust with minimal soot has made it desirable as a cleaner alternative to diesel.[12-15] Importantly, DME can be stored and handled as a liquid, similar to LPG as it forms a liquid phase at pressures above 0.5 MPa, and therefore, can be transported and stored using existing infrastructure.[12] This property makes DME more desirable as a H_2 carrier, as it can produce H_2 through steam reforming and potentially addresses the challenges associated with H_2 transportation and storage.[4]

The catalytic conversion of CO_2 and H_2 to DME requires two unique active sites – (1) a metal oxide for the hydrogenation of CO_2 to methanol (MeOH) (Equation 1 below) and (2) an acid site to dehydrate MeOH to DME (Equation 2).[16] This can be achieved stepwise, via two reactors, known as the indirect method, or simultaneously in one reactor (the direct method) using physical

or hybrid mixtures of the two catalysts.[17] The direct method has been the focus of several studies as it holds specific advantages such as the integration of the reaction into one single-reactor, thus reducing equipment requirements and costs.[18] However, combining two catalysts in one reactor has its own challenges that need to be addressed.

CO_2 hydrogenation:	$CO_2 + 3\,H_2 \rightleftharpoons CH_3OH + H_2O$	$\Delta H = -49.5\ kJ/mol$	(1)
Methanol dehydration:	$2\,CH_3OH \rightleftharpoons CH_3OCH_3 + H_2O$	$\Delta H = -23.4\ kJ/mol$	(2)
Reverse-water gas shift:	$CO_2 + H_2 \rightleftharpoons CO + H_2O$	$\Delta H = +41.2\ kJ/mol$	(3)

In a direct method, the compatibility between the metal oxide and the acidic catalyst is critical as both operate at the same temperature (e.g., 260 °C). Hence, a metal oxide with a good activity for CO_2 hydrogenation, for example at 260°C, should be paired with an acidic catalyst that is active and highly selective to DME at the same temperature.[19, 20] Under the same conditions as DME synthesis, CO_2 can also undergo the reverse-water gas shift (rWGS) reaction (Equation 3), producing carbon monoxide (CO) as a byproduct. This introduces one of the main challenges associated with DME synthesis via CO_2, namely, controlling the yield and selectivity to DME. The endothermicity of the rWGS reaction necessitates the need for low reaction temperatures (e.g., 200 - 260°C) for its suppression to achieve high DME selectivity.[4] However, with low MeOH formation rates at these temperatures, this comes at the cost of decreased DME yields.[15] For this reason, development of a metal oxide catalyst which shows high activity at low reaction temperatures is critical to the success of the pathway. In addition, the stability of the catalyst plays an important role. Due to the formation of water as a byproduct, the catalysts should have good resilience to water and maintain their activity for long hours of operation. Therefore, considering all these factors is important for determining and designing the tandem catalysts for the conversion of CO_2 to DME.

One of the catalysts that is widely used for the hydrogenation of CO_2 is Cu-ZnO-Al_2O_3 (CZA).[21] Cu/ZnO-based catalysts have been shown to be effective for CO_2 hydrogenation to MeOH especially with a structural promoter such as Al_2O_3 which improves reactivity.[22] However, the hydrophilic nature of Al_2O_3 makes it susceptible to poisoning by water formed during the reaction.[23, 24] Recent studies have shown ZrO_2 to be a promising support and promoter that can potentially replace Al_2O_3, resulting to Cu-ZnO-ZrO_2 (CZZ), due to its weaker hydrophilic character which helps inhibit poisoning by water.[25] The Cu/ZrO_2 interfaces in CZZ are said to promote adsorption of CO_2[23] and improve H_2 dissociation and atomic hydrogen (H) spillover which overall results in increased MeOH synthesis activity.[26] Despite the better compatibility of ZrO_2 with Cu/ZnO for the hydrogenation of CO_2, the properties and reactivity of the catalyst still heavily relies on the synthesis methods.

Several studies have tested different synthesis procedures and conditions which resulted in different structures and activities of the generated CZZ catalyst. The precipitation methods, ageing temperature, calcination temperature, and molar composition are some of the parameters that significantly affect the final structure and activity of CZZ. For example, while Raudaskoski et al., using a co-precipitation technique, showed that longer ageing times (24 h) at 80°C after precipitation of CZZ can improve CO_2 conversion and MeOH selectivity,[27] Li et al. showed that calcination temperatures can affect crystallinity and surface composition of CZZ, affecting the catalyst reactivity.[28] Other works have also investigated the effect of Cu/Zn/Zr ratio on the reactivity of CZZ. For example, while Arena et al. reported that CZZ synthesized through the citrate method had the most activity with a Cu:Zn:Zr mole ratio of 2.1:7.2:0.7,[29] Witoon et. al. synthesized CZZ through the reverse co-precipitation method and reported that a 4:3:3 mole ratio

of Cu:Zn:Zr had the most MeOH productivity.[30] Although reactivities similar to CZA have been achieved for CZZ, it is still unclear which set of synthesis conditions (e.g. ageing temperature, calcination temperature, and CZZ composition) results to the highest yield of MeOH.

Meanwhile, the dehydration reaction is typically catalyzed by acid sites present on either alumina (Al_2O_3) or zeolites (e.g., HZSM-5). Particularly, zeolites have been extensively studied for CO_2 to DME conversions as they demonstrate good stability in presence of water (H_2O, a product of methanol synthesis) and high activity even at moderate temperatures (200-260°C).[31] Most studies have focused on using medium-pore and large-pore zeolites such as FER and ZSM-5, respectively.[18, 32-34] However, given the small molecular size of DME, small pore zeolites could also be used without any detrimental effects from steric hinderance. An 8-membered ring zeotype, SAPO-34 (a silicoaluminophosphate), has shown good activity for MeOH dehydration to DME, reaching equilibrium conversions (~88%) even at low temperatures (250°C)[35, 36], which corroborates the potential of SAPO-34 to be applied in direct CO_2 hydrogenation to DME. Nonetheless, to the best of our knowledge, SAPO-34 has not yet been tested for the direct (single reactor) CO_2 to DME conversion. In addition, most studies on the direct CO_2 to DME conversion using tandem catalysts only focus on the laboratory-scale catalytic performance.[31, 33] The economics and carbon footprint analyses of the industrial process are often disconnected from laboratory advances with these studies often performed later, often separately by other research groups.

To that end, in this work, for the first time, we report the activity of a CZZ/SAPO-34 bifunctional system for CO_2 hydrogenation to DME and optimize the parameters and conditions that would maximize the yield of DME. This work reports the following major points: (1) synthesis parameters and composition of CZZ that maximize CO_2 to DME conversion, (2) effect of active

site proximity between the CZZ and SAPO-34, and reaction conditions on the productivity of DME, (3) kinetic model and parameters fitting for the direct CO_2 to DME reactions over a CZZ/SAPO-34 catalytic system, (4) economic factors that drive the CO_2 to DME technology, and (5) a cradle-to-gate carbon footprint analysis of the process considering different feed sources. Notably, we directly investigated the kinetics of the reactions using our experimental data and applied this to a process model to generate an economic and carbon footprint analysis of the process, thereby providing a complete holistic perspective and pointing out possible challenges that this technology may face during scale-up. Taken together, this work provides a holistic picture of the CZZ/SAPO-34 system from its activity in the laboratory-scale up to its application and impacts on an industrial scale.

RESULTS

1. Catalytic Performance of CZZ for MeOH synthesis

The synthesis parameters of CZZ can greatly affect its textural and physicochemical properties which may ultimately affect its ability in converting CO_2 to MeOH. The synthesis method applied in this work utilizes a co-precipitation technique.[27] To optimize the activity of CZZ, synthesis using different ageing (40°C and 80°C) and calcination temperatures (350°C, 500°C, and 600°C) were investigated as these parameters can significantly impact the crystallinity and surface structure of the precipitated catalyst.[26, 27] Based on detailed catalyst testing, an ageing temperature of 40°C and calcination temperature of 500°C resulted in the CZZ with the highest MeOH yield. Details on this can be found in section S2 of the supporting information. The optimum ageing and calcination temperatures were then used in synthesizing CZZ catalysts with varying compositions, which played a major role in the conversion of CO_2 to MeOH. We note that all catalyst evaluation was carried out with negligible mass-transfer limitations (see section S4 in SI).

The different compositions of CZZ and their corresponding MeOH yields were investigated and shown in Table 1. The catalysts are denoted as CZZ-XYZ where X, Y, and Z refers to the molar ratio of Cu, Zn, and Zr, respectively. The Cu:Zn ratio was initially varied among 2:5, 4:3, and 6:1 while maintaining the Zr molar ratio at 3 (CZZ-253, CZZ-433, and CZZ-613, respectively). The Zr content was then adjusted (CZZ-611, CZZ-613, and CZZ-615) with a constant Cu:Zn ratio of 6:1. These range of compositions tested were based on compositions used in previous studies.[28-30, 33, 37] The reactivity of the five unique compositions of CZZ (summarized in **Table S8**) was investigated at 240°C, 500 psig, 18000 mL g_{CZZ}^{-1} h^{-1} and the results are summarized in **Table 1**. Data for reaction temperatures of 220°C, 260°C, and 280°C are also available in **Figure S4**. Across all temperatures, it was observed that MeOH yield goes up with increasing Cu content of CZZ which suggests that Cu plays an important role in MeOH synthesis. To further identify how Cu participates in the reaction, CuO/SiO_2 (at room temperature) and $ZnZrO_x$ support were tested at the same conditions. Both CuO/SiO_2 and $ZnZrO_x$ showed minimal activity for MeOH synthesis implying that Cu on its own is not efficient in producing MeOH and MeOH formation most likely happens in the Cu/Zn and/or Cu/Zr interface, in line with previous works.[23, 26, 38, 39]

Table 1. Properties and catalytic activity (240°C, 500 psig, 18000 mL g_{CZZ}^{-1} h^{-1}) of CZZ with different compositions.

Catalyst	X_{CO_2}[a,*] (%mol_C /mol_C)	S_{MeOH}[b,*] (%mol_C/ mol_C)	MeOH STY[c,*] (mol kg_{cat}^{-1} h^{-1})	d_{CuO}[d] (nm)	S_{BET} (m^2/g)	H_2 consumed[e] (mol H_2/kg_{cat})	CO_2 desorbed[f] (µmol CO_2/g_{cat}) [µmol CO_2/g_{Cu}]
CZZ-253	7.9	44.0	6.9	12.8	84.9	4.0	99.0 [729]
CZZ-433	10.0	37.9	7.6	11.5	73.8	6.6	93.8 [344]
CZZ-611	13.7	39.2	10.8	8.1	59.5	12.8	74.8 [134]
CZZ-613	12.0	37.2	8.9	9.1	71.8	10.5	83.1 [202]
CZZ-615	10.3	41.5	8.6	9.4	82.0	8.5	75.0 [231]
CuO/SiO_2	1.5	37.8	1.1	16.6	143.6	9.3	n.d.[h]
$ZnZrO_x$	0.1	-[g]	0.2	-	48.1	0.9	46.7

[a]CO_2 conversion.

[b]Methanol selectivity.
[c]Methanol space-time yield.
[d]Calculated using the Scherrer equation for the (111) facet of CuO.
[e]Calculated from H_2 TPR.
[f]Calculated from CO_2 TPD.
[g]Only MeOH was detected by the gas chromatograph, but it is possible that a small amount of CO exists which is below the detection limit of the thermal conductivity detector.
[h]Not detected.
[*]Carbon balances were within ±3%.

To explain the reactivity differences, we looked into the powder X-ray diffraction (PXRD) patterns, textural properties, catalyst reducibility, and CO_2 adsorption ability of the calcined catalysts. **Figure 1** shows the PXRD patterns of the CZZ catalysts of different compositions. Peaks for CuO were apparent in all samples, but as Cu loading decreased these peaks became less well defined. Interestingly, ZnO peaks were only visible in samples with the highest Zn loadings (CZZ-253 and CZZ-433) and ZrO_2 peaks were not visible in any CZZ samples, indicating a high dispersion or amorphous phase of Zr. Given that the activity was mostly attributed to Cu, we estimated the crystallite sizes of CuO particles using the Scherrer equation (for the peak of the (111) plane of CuO (2ϑ = 38.8°)). Looking at the crystallite sizes, higher MeOH yields were achieved with smaller CuO crystallite sizes. This is likely due to the increased number of Cu/Zn and Cu/Zr interfaces due to smaller Cu crystallite sizes. The peak associated with CuO broadened with increasing Zr incorporation (CZZ-611 to 615) indicating smaller crystallite sizes for CuO. Furthermore, lower surface areas of CZZ were observed with higher Cu content. However, activity did not appear to vary directly with crystallite size and surface area.

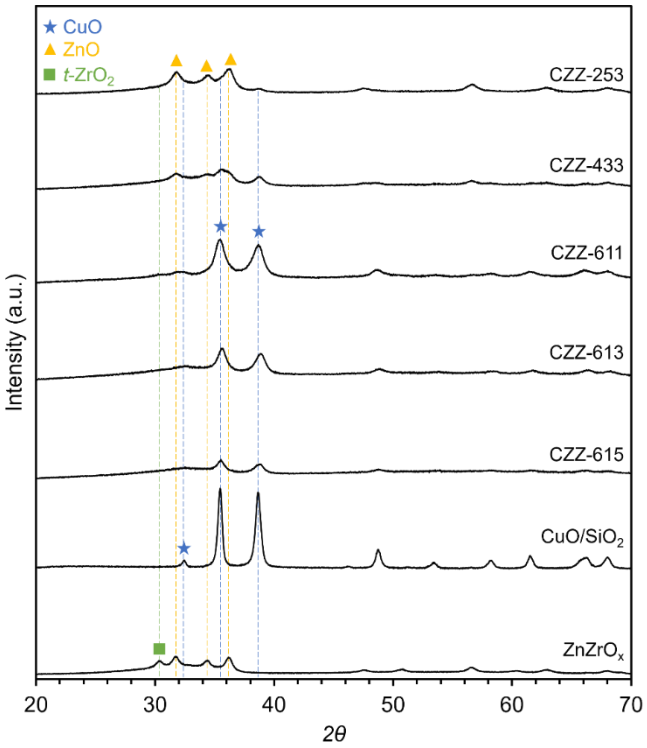

Figure 1. Powder X-ray diffraction (PXRD) patterns of calcined CZZ with different Cu:Zn:Zr molar ratios together with the PXRD pattern of CuO/SiO_2 and $ZnZrO_x$. Blue star, yellow triangle, and green square represent CuO, ZnO, and t-ZrO_2 diffraction peaks, respectively. Catalysts and their compositions (Cu:Zn:Zr:Si %mol/mol) from top to bottom: CZZ-253 (20:50:30:0), CZZ-433 (40:30:30:0), CZZ-611 (75:12.5:12.5:0), CZZ-613 (60:10:30:0), CZZ-615 (50:8.3:41.7:0), CuO/SiO_2 (48.6:0:0:51.4), $ZnZrO_x$ (0:50:50:0). CZZ and $ZnZrO_x$ catalysts were synthesized *via* co-precipitation with an ageing temperature of 40°C and calcination temperature of 500°C. CuO/SiO_2 was synthesized *via* wet impregnation method and followed the same drying and calcination procedures as CZZ.

To characterize the reducibility of the catalysts, H_2 temperature programmed reduction (TPR) was performed on the calcined catalysts as shown in **Figure S5** and the corresponding H_2

consumption are summarized in **Table 1**. A linear correlation between the Cu content of the catalyst and H_2 consumption was observed (**Figure 2A**) with an H_2/Cu molar ratio of ~1.37, which is close to the theoretical value of 1.0 for the reduction of CuO to Cu metal. There is minimal reduction observed for $ZnZrO_x$ implying that the H2 consumption is most likely associated with the reduction of CuO in the CZZ catalyst. The slightly higher H_2/Cu molar ratio could be attributed to the reduction of mixed metallic oxides (e.g., Cu-Zr-O_x) formed at the Cu/Zn and Cu/Zr interfaces, in addition to the partial reduction of $ZnZrO_x$. Taken together, the MeOH yield of CZZ was found to be directly correlated with the reducibility of the catalyst (**Figure 2B**). Catalysts with greater reducibility could indicate the existence of more oxygen vacancies which serve as actives sites for the reaction.[38] However, this does not explain why CuO/SiO_2, which had high reducibility, did not give high MeOH yields. Thus, we performed CO_2 temperature programmed desorption (TPD) (**Figure S6**) and found that Cu supported in SiO_2 did not show significant CO_2 desorption (refer to **Table 1**) which explains its low activity for CO_2 hydrogenation. CZZ catalysts on the other hand showed significant CO_2 adsorption behavior, ranging from 75-100 μmol CO_2/g_{cat}, which demonstrated that the Cu/metal oxide interfaces likely promote the adsorption of CO_2 *(vide infra)* resulting in higher activities. However, the CO_2 adsorption ability of the catalysts was not directly related to Cu content (refer to Table 1 CO_2 desorption values in square brackets) which further proves that some 'synergy' among Cu, Zn, and Zr caused the improvement in MeOH synthesis activity. Examples of these 'synergy' include formation of Cu/Zn or Cu/Zr surface alloys, tuning of H_2 dissociation, change in the adsorption of CO_2, and modification of surface properties such as basicity or defect concentrations which ultimately improves activity to MeOH production.[39] Overall, CZZ-611 had the highest MeOH yield which was used for the tandem catalyst studies.

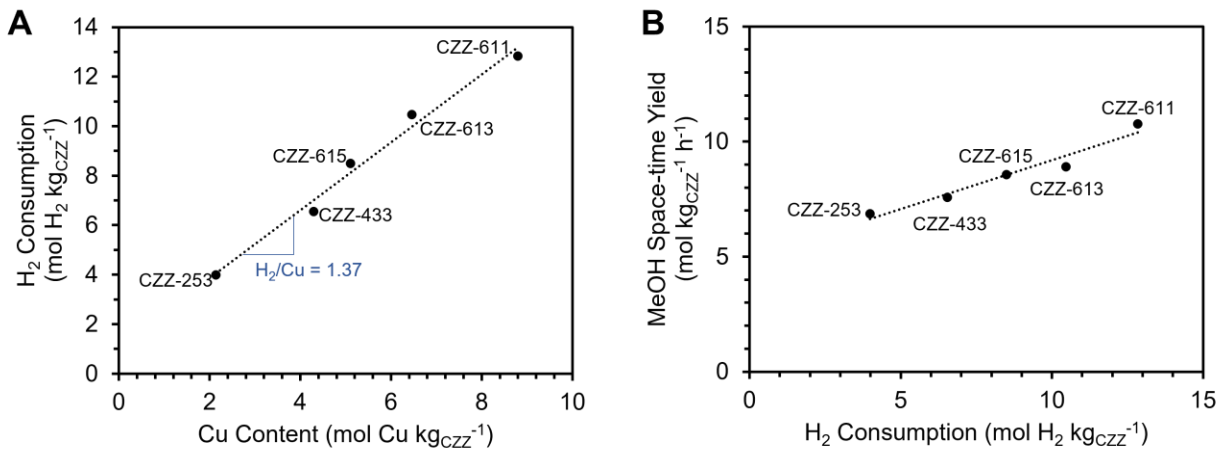

Figure 2. A) H_2 consumption during H_2-TPR (mol H_2 kg_{CZZ}^{-1}) vs Cu content of CZZ catalyst (mol Cu kg_{CZZ}^{-1}). B) Methanol space-time yield (MeOH STY) (mol kg_{CZZ}^{-1} h^{-1}) vs. H_2 consumption during H_2-TPR (mol H_2 kg_{CZZ}^{-1}). The catalysts are denoted as CZZ-XYZ where X:Y:Z refers to the Cu:Zn:Zr molar ratio.

2. Catalytic Performance of CZZ/SAPO-34 Tandem System

2.1. Effect of bed configuration

The catalytic performance of CZZ/SAPO-34 tandem system was initially assessed at a temperature of 260°C, pressure of 500 psig, and GHSV of 18000 mL g_{CZZ}^{-1} h^{-1}. We investigated the performance of CZZ single bed (SB) and four different bed configurations of the tandem system: dual bed (DB), granule-mixed (GM), powder-mixed (PM), and mortar-mixed (MM) (**Figure 3)** which compared how the proximity of the metal and acidic active sites affected the formation of DME.

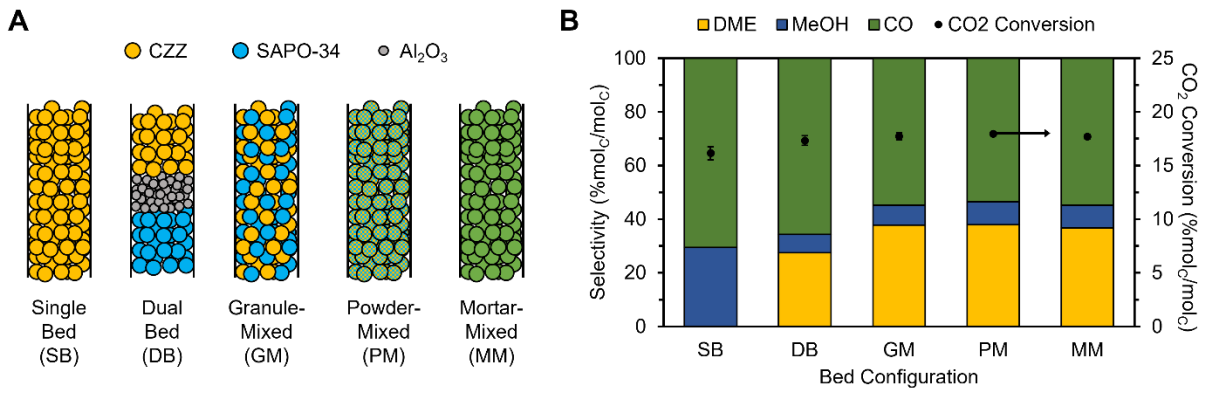

Figure 3. A) Schematic of bed configurations used in the study. From left to right: single bed (SB), dual bed (DB), granule-mixed (GM), powder-mixed (PM), and mortar-mixed (MM). Yellow, blue, and grey spheres refer to CZZ, SAPO-34, and Al_2O_3, respectively. Green spheres refer to the mixture of CZZ and SAPO-34. B) Catalytic performance of CZZ/SAPO-34 tandem system of the different bed configurations. The left axis shows product selectivity (%mol$_C$/mol$_C$) with yellow, blue, and green bars representing DME, MeOH, and CO, respectively. The right axis shows CO_2 conversion (%mol$_C$/mol$_C$) represented by black circles. Reaction conditions: 260°C, 500 psig, 18000 mL g_{CZZ}^{-1} h^{-1}, H_2:CO_2 ratio = 3:1, mass of CZZ = 0.5 g, CZZ:SAPO-34 mass ratio = 1:1. Carbon balances were within ±3% error.

First, we compared the activity of CZZ only (SB) and the DB tandem system. With only CZZ, CO_2 was converted into CO and MeOH *via* the reverse water gas shift (rWGS) and CO_2 hydrogenation, respectively.[40] At 260°C, a CO_2 conversion of ~16% with a MeOH selectivity of ~29% and CO selectivity of ~71% was achieved. Coupling the CZZ with SAPO-34 in a DB configuration resulted in the conversion of MeOH to DME on the acidic sites of SAPO-34 through a dehydration mechanism.[40] A synergetic effect can be observed when the two catalysts are placed together in the bed at 260°C with a slight increase in CO_2 conversion (~17%) and a decrease in

CO selectivity (~66%). The presence of SAPO-34 in the bed increased the overall equivalent MeOH selectivity (MeOH + DME) from ~29% in the SB to ~34% in the DB. Looking at the distribution of MeOH and DME in DB, ~80% of MeOH produced from CZZ was converted into DME suggesting that SAPO-34 functions as an effective dehydration catalyst. With this, a question now arises whether increasing the proximity between the active sites on CZZ and the acidic sites would further improve the yield of DME.

We investigated the activity at bed configurations which have closer proximity of active sites by mixing CZZ and SAPO-34 as pellets (GM) or powders (PM and MM). The PM and MM configurations have roughly the same active site distances but only varied in the preparation method. PM uses a lightly mixed catalyst mixture unlike the mortar-mixed catalyst mixture (MM) which grinded the catalysts, allowing solid-state ion-exchange of metal ions with the Brønsted acid sites of SAPO-34.[41] At 260°C, GM, PM, and MM configurations had DME + MeOH selectivity of ~46%, higher than the DME + MeOH selectivity from DB configuration (~34%) at the same CO_2 conversions (~18%). This suggests that the close contact of the active sites between CZZ and SAPO-34 in GM, PM, and MM improved the yield to DME and MeOH. This could be due to the faster transfer of intermediates between the active sites of CZZ and SAPO-34, allowing faster conversions of methanol and shifting the equilibrium towards further MeOH and DME production.[42] When comparing the results among GM, PM, and MM, the closer proximity of active sites did not show changes in activity, suggesting that the transfer of intermediates (between active sites and inside the catalyst) in GM does not limit the reaction. It is to be noted that previous works have reported reduced activity at very close proximity (MM) owing to the ion exchange of metal cations with the acidic sites of the zeolite which were not observed in our results, likely due to the

lower reaction temperature employed in this study.[42, 43] Due to the enhanced selectivity to DME with GM configuration and no further improvements with PM and MM, GM was chosen for further parametric studies.

2.2. Parametric Studies

In order to determine conditions that maximize the DME yield of the CZZ/SAPO-34 tandem system, temperature, pressure, GHSV, H_2:CO_2 ratio, and CZZ:SAPO-34 mass ratio were varied. **Figure 4** shows the activity of the tandem system at different varied parameters.

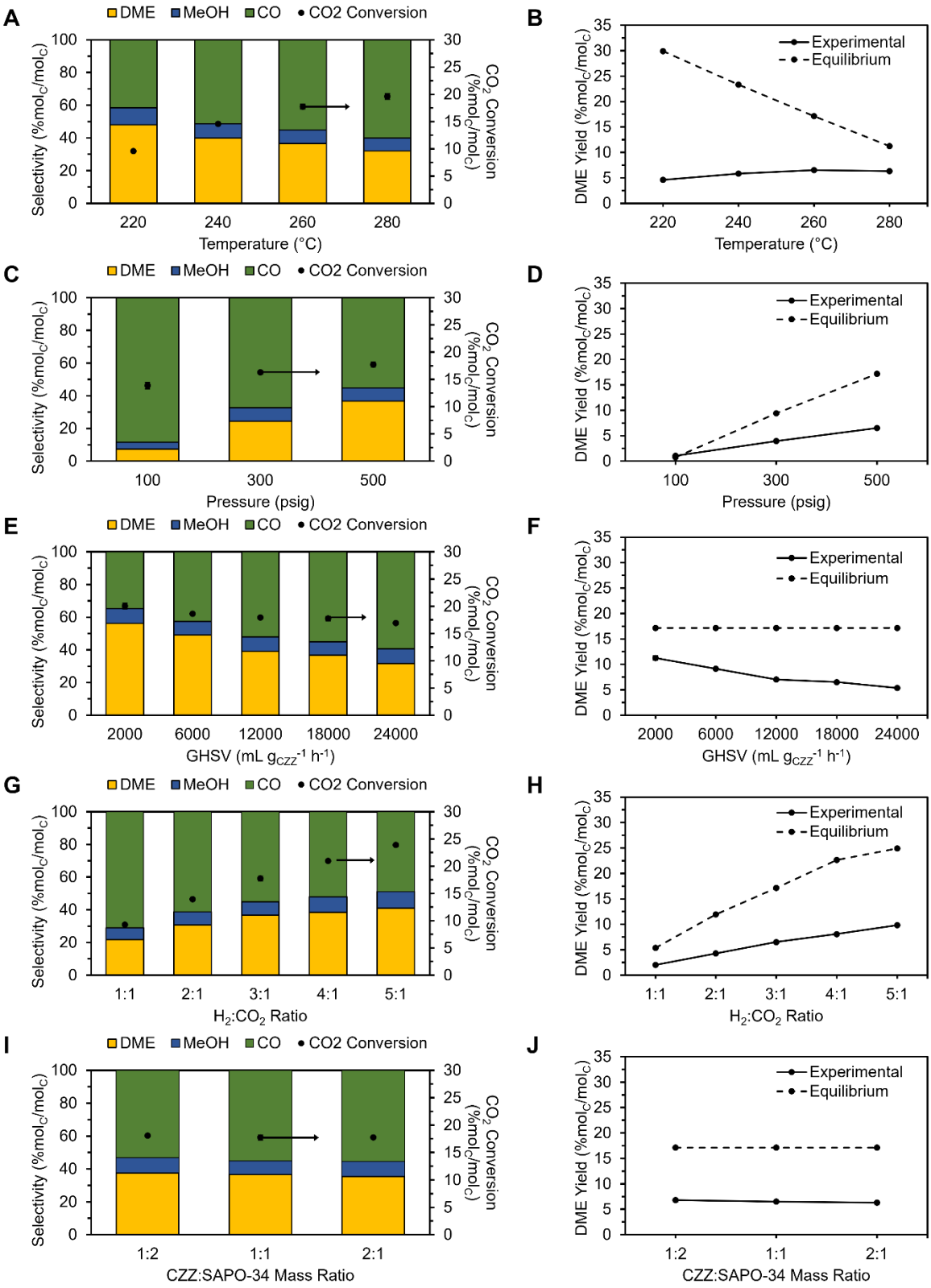

Figure 4. Catalytic performance of CZZ/SAPO-34 at varied A,B) temperature (220, 240, 260, 280°C), C,D) pressure (100, 300, 500 psig), E,F) H_2:CO_2 ratio (1:1, 2:1, 3:1, 4:1, 5:1), G,H) GHSV (2000, 6000, 12000, 18000, 24000 mL g_{CZZ}^{-1} h^{-1}), and I,J) CZZ:SAPO-34 mass ratio (1:2, 1:1, 2:1). For Figures A, C, E, G, and I, the left axis shows product selectivity (%mol_C/mol_C) with yellow, blue, and green bars representing DME, MeOH, and CO, respectively. The right axis shows CO_2 conversion (%mol_C/mol_C) represented by black circles. For Figures B, D, F, H, and J, the solid line shows DME yield from experimental data while dashed lines show equilibrium DME yield. Base reaction conditions: 260°C, 500 psig, 18000 mL g_{CZZ}^{-1} h^{-1}, H_2:CO_2 ratio = 3:1, mass of CZZ = 0.5 g, CZZ:SAPO-34 mass ratio = 1:1, GM configuration. Carbon balances were within ±3% error.

Performing the reaction at an appropriate temperature is important to maximize DME yield due to competition with the rWGS reaction. Looking at the effect of temperature (**Figure 4A**), increased CO_2 conversions (~10% at 220°C and ~20% at 280°C) were observed at increasing temperatures although CO selectivity (~42% at 220°C and ~60% at 280°C) became favorable due to the endothermic nature of the rWGS reaction. In contrast, MeOH and DME selectivity dropped due to the exothermicity of the CO_2 hydrogenation and MeOH dehydration reactions.[4, 14, 40] Hence, the right balance among temperature, CO_2 conversion, and DME selectivity must be considered to obtain optimum DME yields. Results showed that a reaction temperature of 260°C produced the most DME (**Figure 4B**) for the CZZ/SAPO-34 system at the base reaction conditions.

Higher CO_2 conversion and DME selectivity were observed with increased reaction pressure, (**Figure 4C,D**) and H_2:CO_2 ratio (**Figure 4E,F**) which agrees with the thermodynamics of CO_2 to DME conversion (**Equations 1-3**).[14, 44] The overall CO_2 to DME reaction involves 8 moles of reactant with only 4 moles of product indicating that high pressure favors DME formations per Le Châtelier's principle. Similarly, the effect of H_2:CO_2 ratio can be explained by Le Châtelier's principle. The stoichiometric ratio of H_2:CO_2 for CO_2 to DME conversions is 3:1. Thus, an H_2-rich feed favors the formation of products while an H_2-lean feed supports the selectivity to CO.[14]

On the other hand, varying the GHSV (**Figure 4G,H**) resulted in an opposite trend compared to pressure and H_2:CO_2 ratio. As the GHSV was decreased, a rise in CO_2 conversion (~17% at 24000 mL g_{CZZ}^{-1} h^{-1} to ~20% at 2000 mL g_{CZZ}^{-1} h^{-1}) was observed with improved DME selectivity (~32% at 24000 mL g_{CZZ}^{-1} h^{-1} to ~56% at 2000 mL g_{CZZ}^{-1} h^{-1}). Lower GHSV increases the residence time, allowing the system to reach its equilibrium concentrations and resulting in increased conversion and DME yield. Meanwhile, adjusting the mass ratio of CZZ:SAPO-34 resulted in minimal changes in performance (**Figure 4I**) and DME yield (**Figure 5J**). This suggests that MeOH dehydration in SAPO-34 is likely fast and that the MeOH formation is controlling the kinetics of the CO_2 to DME reaction.

2.3. Stability Test

We next studied the activity of CZZ/SAPO-34 for long time-on-stream (50 h) using optimized conditions from the parametric studies (260°C, 500 psig, 2000 mL g_{CZZ}^{-1} h^{-1}, H_2:CO_2 ratio = 3:1, mass of CZZ = 0.5 g, CZZ:SAPO-34 mass ratio = 2:1, GM configuration) to investigate the

stability of the catalyst, as shown in **Figure 5**. Minimal changes in CO_2 conversion (~20%) and CO selectivity (~34%) were observed for 50 h. DME selectivity decreased slightly from ~60% to ~56% after 14 h and remained consistent until 50 h. Consequently, MeOH selectivity increased from ~4% to ~10% after 9 h and stayed constant until 50 h. Initial DME and MeOH selectivity changes could be attributed to SAPO-34 reaching steady-state in the first 14 h. Looking at the thermo-gravimetric analysis (TGA) of the spent SAPO-34 (**Figure S9**), there was no discernible difference when compared with the TGA of pre-treated SAPO-34 indicating minimal coke formation. This shows that SAPO-34 has the potential to be a high performing and stable acid catalyst for CO_2 to DME reactions.

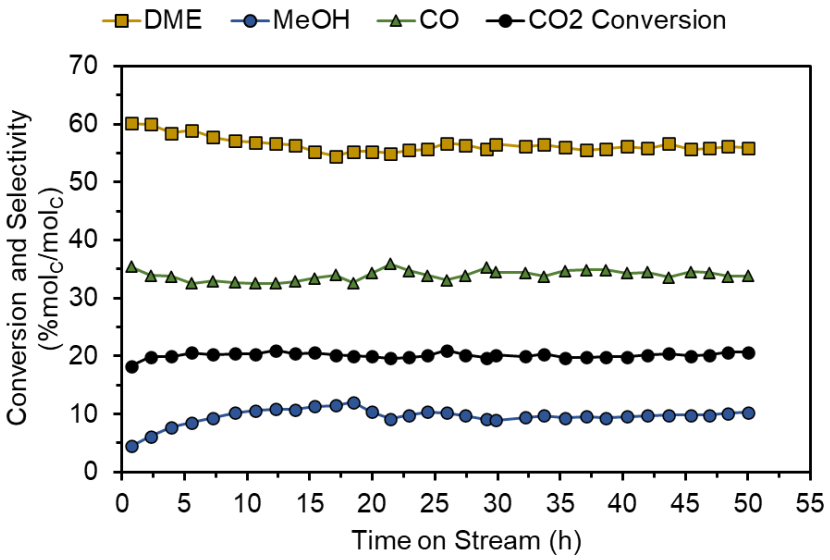

Figure 5. Performance of CZZ/SAPO-34 for CO_2 hydrogenation to DME for 50 h of operation. Yellow squares, blue circles, and green triangles represent DME, MeOH, and CO selectivity ($\%mol_C/mol_C$), respectively, while black circles show CO_2 conversion ($\%mol_C/mol_C$). Reaction

conditions: 260°C, 500 psig, 2000 mL g_{CZZ}^{-1} h^{-1}, H_2:CO_2 ratio = 3:1, mass of CZZ = 0.5 g, CZZ:SAPO-34 mass ratio = 2:1, GM configuration.

Overall, tests on the optimization of CZZ showed that CZZ-611 synthesized with an ageing temperature of 40°C and calcination temperature of 500°C had the highest yield for MeOH. When coupled in a tandem configuration with SAPO-34, optimum DME yields can be attained by using a granular-mixed (GM) configuration operated at 260°C, 500 psig, 2000 mL g_{CZZ}^{-1} h^{-1}, H_2:CO_2 ratio = 3:1, mass of CZZ = 0.5 g, and CZZ:SAPO-34 mass ratio = 2:1.

3. Kinetic Model Fitting

To develop a process model as the basis for a techno-economic analysis (TEA), a kinetic model would need to be established for the CZZ/SAPO GM system to account for changes in feed composition following the implementation of recycle streams in the model *(vide infra)*. To do this, experimental data from the parametric studies were fitted against an existing kinetic model[32]. Details on the kinetic model and the fitting can be seen in section S1.5 of the SI. The fitting was done by minimizing an objective function (χ^2) which computes the difference between the computed value and experimental data (**Equation S14**). The resulting kinetic model fitted well with experimental data as shown in **Figure S10** with a χ^2 of 9.8. The tabulated kinetic parameters are shown in **Table 4**. Most of the errors of the fitted model were associated with MeOH selectivity as seen in the parity plot (**Figure 6**). The errors could be attributed to product streams with low MeOH concentrations as these streams had higher measurement inaccuracies due to a smaller gas-chromatograph peak area. Nonetheless, the kinetic model was used to simulate data at high DME yields and low MeOH concentrations such that the deviations of MeOH from the kinetic model were deemed acceptable for the techno-economic analysis.

Table 4. Estimated kinetic parameters based on the training set.

Parameter	Unit	Estimated Value
A_1	-	24.36
A_2	-	16.92
A_3	-	-0.27
$E_{A,1}$	kJ/mol	84.44
$E_{A,2}$	kJ/mol	76.93
K_1	$bar^{-1.5}$	4.98
K_2	$bar^{-0.5}$	376.69
K_3	bar^{-1}	1.57

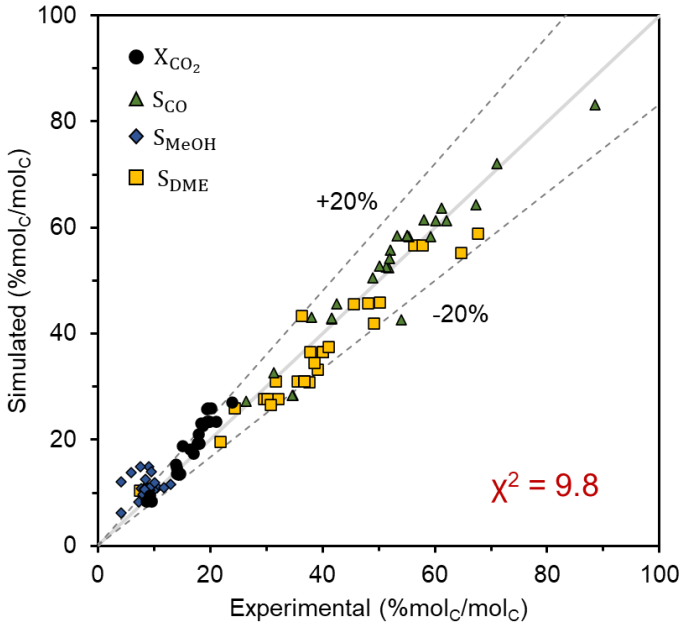

Figure 6. Parity plot comparing experimental data and simulated results from the fitted kinetic model. Yellow squares, blue circles, and green triangles represent DME, MeOH, and CO selectivity (%mol$_C$/mol$_C$), respectively, while black circles show CO_2 conversion (%mol$_C$/mol$_C$). The dotted lines represent ±20% error.

4. Techno-economic analysis (TEA)

4.1. Technical Analysis

Using the fitted kinetic model and optimized reaction conditions from parametric studies, a process simulation for a CO_2 to DME plant (process flow diagram, PFD in **Figure 7**) with 20,000 tons per year (tpy) capacity was designed in Aspen Plus v14. CO_2 (S1) and H_2 (S2) entered the plant and were compressed to 35 bar. These were then mixed with the unreacted gas recycle stream (S30), which was heated to 260°C before going into the packed bed reactor (PBR1). The product gases then proceeded to a series of separation processes. The bulk of unreacted H_2 and CO_2 were separated through a flash drum (F1) in S14, which was recycled back to the reactor. Meanwhile, products such as MeOH, DME, and water went into S15, which was directed to three distillation columns for separating and purifying DME and MeOH. In the first column (DT1), unreacted gases, CO, and DME were recovered at the top (S18) while MeOH and water were collected at the bottom of the column (S19). S18 went to the second column (DT2), which purified DME (>99.9% purity) into S21 while the rest of unreacted gases and CO were recycled back to the reactor (S20). In parallel, S19 was directed to the third column, which separated and purified MeOH (>99.5% purity) at the top of the column (S23) and water (>99.4% purity) at the bottom (S24).

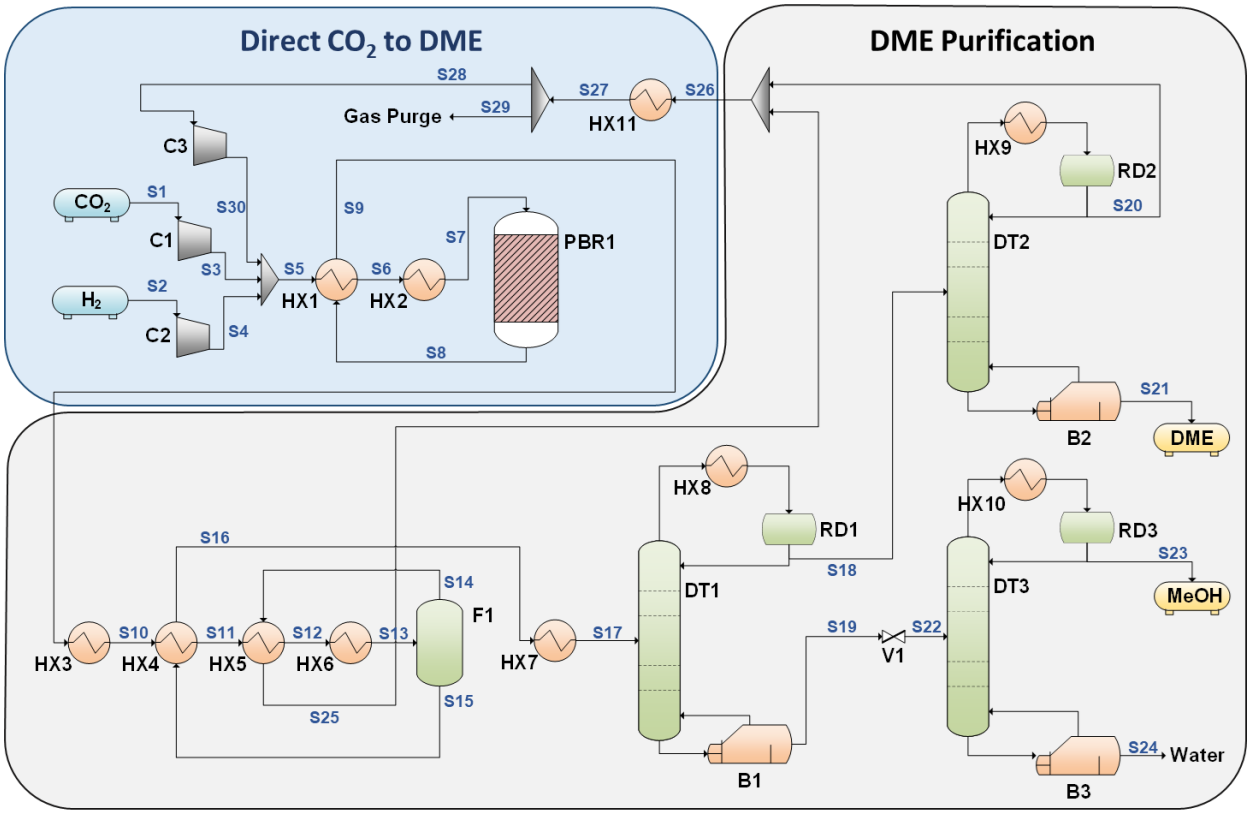

Figure 7. Process flow diagram (PFD) for the one-step CO_2 hydrogenation to DME. Utilities streams are omitted.

A summary of the technical performance indicators can be found in **Table 5**. The single-pass CO_2 conversion (20.4%) and DME selectivity (55.3%) of the process model were similar to those observed in the laboratory-scale stability test performed for CZZ/SAPO-34 (X_{CO2} = 20% and S_{DME} = 56%) operated under the same conditions (see Section 2.3). This validated the successful incorporation of the experimental data into the process model through the developed kinetic model. Recycling the unreacted gases resulted in an overall CO_2 conversion of 96.2% and a DME selectivity of 75.8%, which was close to the equilibrium distribution between DME (78.4%) and methanol (21.6%). The higher overall selectivity of DME compared to the per-pass selectivity was

likely due to the recycling of CO and its further conversion into MeOH and DME. At steady state, the recycle-to-feed ratio was 4.0 for H_2 and 3.7 for CO_2. A conversion factor of 0.4 was obtained which indicates that for every 1 kg of CO_2 fed into the plant, 0.4 kg of DME was generated (76.5% of theoretical maximum yield).

Table 5. Performance indicators of the designed CO_2 to DME plant.

Performance Indicator	Value	Unit
Per pass CO_2 conversion	20.4	$\%mol_C/mol_C$
Per pass DME selectivity	55.3	$\%mol_C/mol_C$
Overall CO_2 conversion	96.2	$\%mol_C/mol_C$
Overall DME selectivity	75.8	$\%mol_C/mol_C$
H_2 feed	6.9	kton/y
CO_2 feed	50.4	kton/y
H_2 recycle-to-feed ratio	4.0	kton/kton
CO_2 recycle-to-feed ratio	3.7	kton/kton
DME productivity	20.0	kton/y
Conversion factor	0.4	kton DME/kton CO_2

4.2. Economic Analysis

From the process simulation in Aspen Plus v14, an economic analysis was performed using Aspen Process Economic Analyzer (APEA). The total estimated purchased equipment cost (PEC) amounted to $13.7M with the distribution shown in **Figure 8A**. A major portion was associated with the cost of compressors (58%) followed by the packed bed reactor (24%). Heat exchangers and distillation towers corresponded to 5% and 3% of the PEC, respectively. Flash drums, pumps, and turbines only accounted for ~1% of the PEC. Lastly, equipment (boiler and cooling tower) for generation of utilities contributed 9% of the PEC. A total CAPEX of $81.5M was estimated for a 20,000 tpy capacity CO_2 to DME plant. The complete components of the CAPEX can be found in **Table S7**.

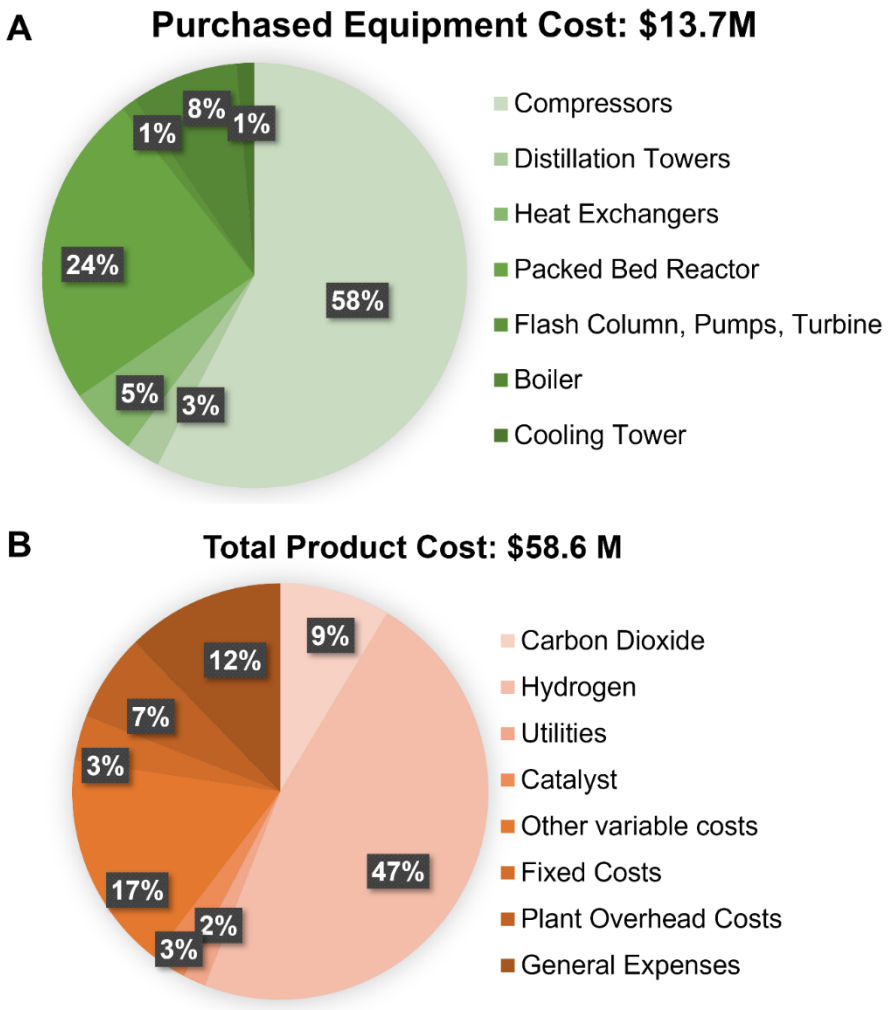

Figure 8. A) Breakdown of purchased equipment cost (PEC) obtained from Aspen Plus v14's Aspen Process Economic Analyzer (APEA). B) Breakdown of operational expenditure (OPEX) based on raw material, utility, and catalyst usage, and other variable and fixed costs estimated based on OPEX factors.[45]

An annual operational expenditure (OPEX) of $58.6M was estimated for a 20,000 tpy capacity CO_2 to DME plant. The breakdown of the OPEX was depicted in **Figure 8B**. A significant portion of the OPEX came from the cost of H_2 (47%) while CO_2 only accounted for 9%. Utilities and catalysts constituted 2% and 3% of the OPEX, respectively. The rest of the OPEX is comprised of

other variable costs (i.e. operating labor and supervision, operating supplies, laboratory charges, royalties), fixed costs (i.e. taxes, insurance), plant overhead costs, and general expenses (i.e. administrative costs, distribution and marketing, research and development) estimated through OPEX factors.[45]

To better understand the economics of CO_2 to DME processes, we computed the annual DME production cost (ADPC) and minimum DME selling price (MDSP) as summarized in **Table 6**. The ADPC amounted to $66.6M and was mostly dominated by the OPEX (~88%) with CAPEX constituting only a small portion (~12%). The calculated MDSP was $3.21/kg. Comparing it with the current value of DME which is $0.88/kg, DME from CO_2 was roughly 3.6 times more expensive. Even so, it is best to note that the process comes with decreased CO_2 emissions, which is important to consider in the oncoming years, especially with the worsening effects of global warming. In addition, the production cost of DME was mostly from operation costs wherein a near majority comes from the supply of H_2. This signifies the importance of lowering H_2 prices in decreasing the production cost of DME from CO_2.

Table 6. Economic indicators of the designed CO_2 to DME plant.

Economic indicators	**Value**	**Unit**
CAPEX	81.5	$M
Annualized CAPEX ($CAPEX_{Annual}$)	8.0	$M
OPEX	58.6	$M
Annual DME Production Costs (ADPC)	66.6	$M
Minimum DME Selling Price (MDSP)	3.21	$ kg^{-1}

Based on the MDSP, DME from CO_2 hydrogenation is not yet economically competitive with DME from natural gas. However, commodity prices fluctuate over time and vary significantly depending on the source/industry where they are obtained from. Hence, a sensitivity analysis on MDSP (**Figure 9**) was performed to get insights into how these changes affect the cost of DME. We also investigated the effect of changes in CAPEX, tax and interest rates, and catalyst lifetime.

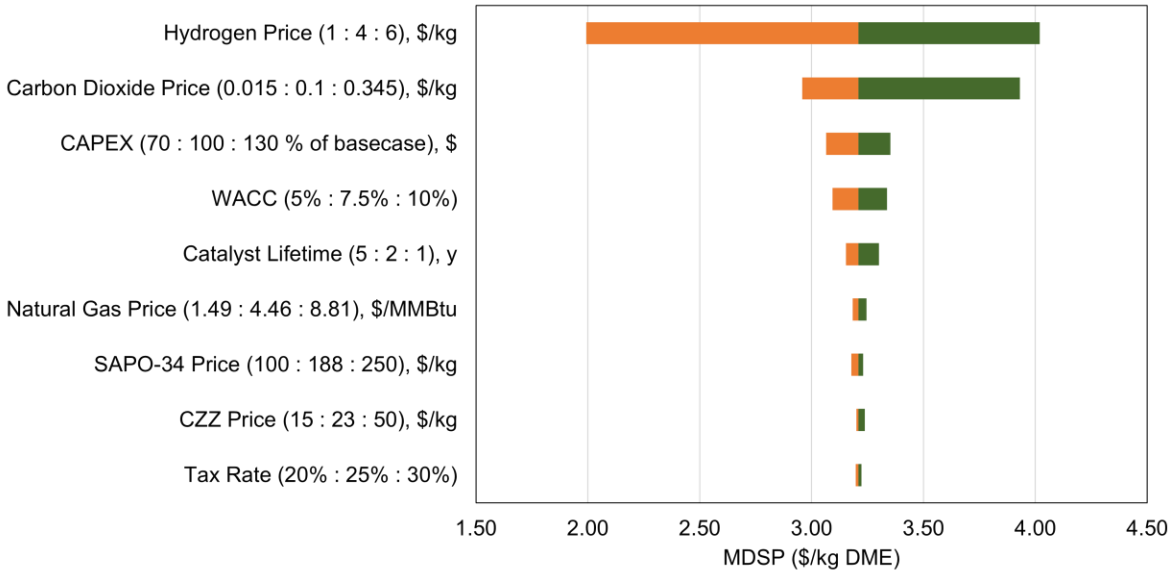

Figure 9. Effect of the different cost factors on the minimum DME selling price (MDSP) of the direct CO_2 hydrogenation to DME.

The cost of hydrogen had the most impact on MDSP. Even with the use of the cheapest hydrogen from natural gas (grey hydrogen, \$1-2/kg[46, 47]), the MDSP only lowers to ~\$1.99/kg, still higher than the current value of DME (\$0.88/kg). The cost of CO_2 also had notable effects on MDSP. The price of captured CO_2 can vary among industries and is affected by factors such as the volume,

CO_2 concentration, and pressure of exhaust gases in a plant.[48] Utilization of captured CO_2 from natural gas processing, which has a cost of \$0.015-0.025/kg CO_2[49], could reduce the MDSP to as low as ~\$2.96/kg while the use of the more expensive CO_2 directly captured from air (\$0.135-0.345/kg CO_2)[48] could result in MDSP as high as ~\$3.93/kg. The CAPEX, interest rates and catalyst lifetimes were observed to substantially affect the MDSP, resulting in a change ranging from ~\$3.07/kg to ~\$3.35/kg. Utility cost, catalyst cost, and tax rate had a small impact on MDSP. Overall, the sensitivity analysis highlights that the economics of CO_2 hydrogenation to DME is mainly driven by hydrogen costs, further emphasizing the importance of reducing green hydrogen costs.

4.3. Carbon footprint

The CO_2 to DME plant is desired to have zero or negative overall CO_2 emission. Thus, we looked into the cradle-to-gate carbon footprint (kg CO_2 eq/kg DME) of the CO_2 to DME plant and how it changes with varying H_2, CO_2, and boiler energy sources as depicted in **Figure 10**. The cradle-to-gate analysis covers emissions from the acquisition of raw materials until the point it leaves the CO_2 to DME plant gate. As a base case, H_2 was assumed to come from electrolyzers powered by renewable energy (0 kg CO_2 eq/kg DME), CO_2 was captured from an external industrial plant (0 kg CO_2 eq/kg DME), and the steam boiler was powered by natural gas (0.37 kg CO_2 eq/kg DME). CO_2 captured from an external plant was considered to have an emission of zero as it has not entered nor come from the atmosphere. At these assumptions, the total CO_2 footprint of the base case is 0.21 kg CO_2 eq/kg DME, which includes the emitted greenhouse gases (GHGs) from the process purge line having an equivalent emission of 0.08 kg CO_2 eq/kg DME.

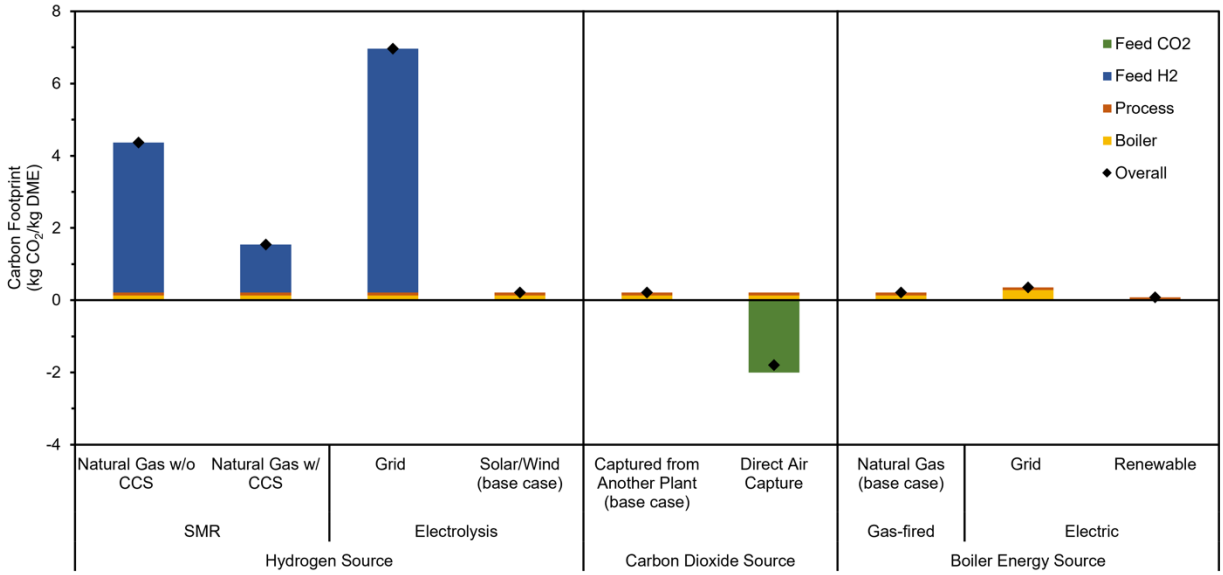

Figure 10. Effect of varying H_2 source, CO_2 source, and boiler energy source on the carbon footprint of the CO_2 to DME plant. Green, blue, orange, and yellow bars represent equivalent CO_2 emissions from feed CO_2, feed H_2, process emissions, and steam boiler, respectively, while the black diamond shows the overall CO_2 emissions.

Among the three variables investigated, H_2 had the most impact on the overall carbon footprint of the CO_2 to DME process. Steam methane reforming (SMR) of natural gas for H_2 production (grey H_2) releases significant amounts of CO_2 (12 kg CO_2 eq/kg H_2)[47]. When used as a hydrogen source, the total footprint rose to 4.4 kg CO_2 eq/kg DME. However, when SMR is coupled with CCS at 93% capture rate (blue H_2), the carbon footprint can be significantly reduced to 1.5 kg CO_2 eq/kg DME. Surprisingly, utilizing hydrogen from electrolyzers that rely on electricity from the grid led to a higher carbon footprint (7.0 kg CO_2 eq/kg DME) due to the high electricity demand of current electrolyzers and the fact that a major portion (~60%) of electricity from the grid comes from natural gas and coal.[50] On the other hand, changing the CO_2 source to direct air capture

(DAC) resulted in a negative carbon footprint of -1.8 kg CO_2 eq/kg DME as CO_2 is directly removed from air and converted to DME. However, it is important to note that these are only cradle-to-gate emissions. When considering DME consumption, GHG emissions should be captured and prevented from entering the atmosphere to maintain a negative emission on a cradle-to-grave basis. Going back to the base case, a significant contributor to the carbon emissions comes from the steam boiler. Using electric boilers powered by the grid resulted to higher footprint (0.36 kg CO_2 eq/kg DME) relative to the base case while using renewable energy led to a minimal emission of 0.08 kg CO_2 eq/kg DME.

DISCUSSION

To summarize, we determined the ageing temperature (40°C), calcination temperature (500°C), and composition of CZZ (611) that gave the highest MeOH yield. We then looked into the performance of CZZ/SAPO-34 and optimized its conditions (260°C, 500 psig, 2000 mL g_{CZZ}^{-1} h^{-1}, H_2:CO_2 ratio = 3:1, mass of CZZ = 0.5 g, and CZZ:SAPO-34 mass ratio = 2:1, GM configuration) to favor DME yield. Through the development of kinetic and process models, we evaluated the economics and environmental footprint of the process, considering a DME plant capacity of 20,000 tpy, wherein we identified the feed hydrogen source to significantly affect the economics and cradle-to-gate carbon footprint of the process.

From the catalyst evaluation studies, the investigation on the ageing and calcination temperatures have revealed that ageing at 40°C and calcination at 500°C resulted in the CZZ structure with the highest MeOH yield. Several studies on CZZ performed ageing at 80°C - 90°C and calcination at 300 - 400°C but did not report whether these conditions were optimized or adapted from a previous

study.[27, 28, 30, 51] This work points out the importance of performing synthesis optimization to generate results that fully exhibit the potential of the catalyst synthesized. In terms of composition, CZZ-611 had the highest activity, which is likely due to the increased number of Cu sites, generally considered as the active phase of the catalyst[52], and higher Cu/ZnO and/or Cu/ZrO_2 interfaces and higher activity. Our results suggest that Cu/metal oxide interfaces are critical to the hydrogenation of CO_2 as Cu on its own is not efficient in producing MeOH. The direct contact between Cu metal and the basic sites of ZnO may favor the formation of Cu/Zn alloys, which have been shown to provide dual binding sites for the activation of CO_2 and catalyze its hydrogenation.[53, 54] Meanwhile, ZrO_2 has been suggested to interact with metallic Cu, which creates active sites for the selective reaction to MeOH and helps in increasing MeOH selectivity.[39, 55] The combination of these synergetic effects likely resulted in a high MeOH yield in this study. We note that the optimum composition of CZZ (71 wt.% Cu and 12 wt.% Zn) determined in this work is close to commonly used composition of CZA used industrially (50-70% wt.% Cu and 20-50 wt.% Zn)[21, 38, 56, 57].

We then paired the optimized CZZ-611 with SAPO-34 and showed the capability of SAPO-34 to be utilized in the direct hydrogenation of CO_2 to DME. Different reactivities at different proximities of the CZZ and SAPO-34 active sites demonstrated the importance of a proper bed configuration in tandem systems. Mixing CZZ with SAPO-34 creates a synergy wherein MeOH (from CZZ) is immediately consumed in SAPO-34 which effectively lowers instantaneous concentrations of MeOH in the system and by Le Châtelier's principle pushes the reaction to produce more MeOH and eventually DME. Thus, the increased proximity between active sites hastens the consumption of the intermediate and improves the 'synergetic effect' as observed in the experiments conducted. However, no improvements were observed between GM and PM/MM, which denotes that the reaction is not mass transfer limited but rather kinetically controlled. In all

tests, SAPO-34 effectively converted MeOH to DME at the temperature range tested (220°C - 280°C), reaching near equilibrium distributions between MeOH and DME. In addition, SAPO-34 showed 100% selectivity to DME and displayed exceptional stability and no signs of deactivation for long hours (50 h) of operation demonstrating its excellent applicability in CO_2 to DME conversions. We like to acknowledge that the optimum operating conditions identified in this study (260°C, 500 psig, 2000 mL g_{CZZ}^{-1} h^{-1}, H_2:CO_2 ratio = 3:1, mass of CZZ = 0.5 g, CZZ:SAPO-34 mass ratio = 2:1) are restricted by operational limitations in the laboratory. Higher CO_2 conversions and DME selectivity could ideally be further achieved by performing the reaction at higher pressures and lower GHSV.

Economic analysis of a 20,000 tpy DME plant showed that the industrial feasibility of CO_2 hydrogenation to DME are highly reliant on raw material prices, especially H_2. Assuming the use of green H_2 and captured CO_2 from industrial plants, an MDSP of $3.21/kg DME was identified and has minimal cradle-to-gate carbon footprint (0.21 kg CO_2 eq/kg DME). A lower MDSP of $1.99/kg DME was estimated when using H_2 sourced from steam methane reforming. However, this comes at the cost of a high carbon footprint (4.4 kg CO_2 eq/kg DME). Clearly, there is an inverse relationship between the cost of producing DME and carbon footprint. Low DME production costs with low CO_2 emissions rely on the development of cheaper green H_2 technologies. According to a study by Detz et al.[58], green H_2 costs will be competitive with grey H_2 between 2025 and 2048 in an optimistic scenario. However, current green H_2 costs still range from $3.5/kg H_2 - $5/kg H_2[47] signifying that it will not be competitive with grey H_2 anytime soon. Even when assuming low H_2 ($1/kg H_2) and CO_2 ($0.015/kg H_2) prices, MDSP only lowers to ~$1.74/kg DME which is still ~2x more expensive than current DME prices ($0.88/kg). Hence,

further development in CO_2 hydrogenation technologies and increased catalyst efficiencies are also critical in making the technology feasible.

CONCLUSION

In this work, a multipronged approach was taken to study CO_2 hydrogenation to DME using tandem CZZ/SAPO-34 catalysts, from optimizing the catalytic performance to an assessment of its economic viability and environmental impact resulting from the catalytic advances. CZZ-611 synthesized at an ageing temperature of 40°C and calcination temperature of 500°C resulted to the highest activity for CO_2 to MeOH reaction, reaching CO_2 conversion of 13.7% and MeOH selectivity of 39.2% at 260°C, 500 psig, and 18000 mL g_{CZZ}^{-1} h^{-1}. For the first time, we coupled CZZ with SAPO-34 in a tandem catalytic system which effectively performed CO_2 hydrogenation to DME. We observed that increased proximity (e.g., GM, PM, and MM configuration) of the active sites improved the CO_2 conversion and DME selectivity. In addition, high DME yields can be obtained at a temperature of 260°C, high pressures (e.g. 500 psig, 700 psig), low GHSV (e.g. 2000 mL g_{CZZ}^{-1} h^{-1}), and high H_2:CO_2 ratios (e.g. 3:1, 4:1, 5:1). On the other hand, varying CZZ:SAPO-34 mass ratios from 1:2 to 2:1 did not show significant changes in activity. The CZZ/SAPO-34 tandem system shows good stability for 50 h with a CO_2 conversion of 20% and DME selectivity of 56%.

An experimental data-fitted kinetic model was developed for CZZ/SAPO-34 tandem system and applied to a process simulation to perform a techno-economic analysis (TEA) on a 20,000 tpy capacity plant. TEA revealed that DME production cost was highly dependent on feedstock cost

(H_2 and CO_2) rather than catalytic or operational variables. A minimum DME selling price (MDSP) of $3.21/kg was computed for the base case which could be reduced to $1.99 /kg if H_2 costs lower to $1/kg. The CO_2 to DME plant had a carbon footprint of 0.21 kg CO_2 eq/kg DME, for the base case, which is greatly influenced by the type of hydrogen used. A negative CO_2 emission of -1.6 kg CO_2 eq/kg DME could be achieved when using CO_2 captured from air. Using CO_2 captured from other processes or plants only results in a nearly carbon-neutral DME production process. In sum, the economic and environmental impacts of a CO_2 to DME plant are largely driven by the feedstock, hydrogen, and is, therefore, reliant on the development of cheaper green hydrogen technologies to make DME from CO_2 more cost-effective and sustainable. Overall, this work gave a holistic view of the challenges of CO_2 hydrogenation from catalyst design and synthesis up to scale-up and industrial operation.

AUTHOR INFORMATION

Corresponding Author

*Email. manish.shetty@tamu.edu

Author Contributions

The manuscript was written through the contributions of all authors. All authors have given approval for the final version of the manuscript. ‡These authors contributed equally.

SUPPORTING INFORMATION

Experimental, kinetic, process modelling, economic analysis, and carbon footprint analysis methods, ageing and calcination studies, PXRD patterns, H_2-TPR profiles, CO_2-TPD profiles, additional reactivity, test on mass transfer limitation, thermogravimetric analysis, kinetic model data, detailed process model description and process streams data, and OPEX estimation methods are included in the supporting information.

ACKNOWLEDGEMENT

This work was supported by Texas A&M University (TAMU), Texas A&M Engineering Experiment Station (TEES), and National Science Foundation (NSF) CBET grant number 2245474. J. V. acknowledges support from Dr. Dionel E. Avilés '53 and Dr. James E. Johnson '67 Graduate Fellowship at Texas A&M University and the NSF Graduate Research Fellowship for support. N.S. acknowledges support from the Royal Thai Government Fellowship. M.S. acknowledges support from the Development Fellowship awarded by the National Laboratories Office (NLO) at the Texas A&M University System. J.M. acknowledges support from the Artie McFerrin Department of Chemical Engineering and College of Engineering at TAMU for assistantship and fellowship awards.

REFERENCES

(1) Jones, M. W.; Peters, G. P.; Gasser, T.; Andrew, R. M.; Schwingshackl, C.; Gütschow, J.; Houghton, R. A.; Friedlingstein, P.; Pongratz, J.; Le Quéré, C. National contributions to climate change due to historical emissions of carbon dioxide, methane, and nitrous oxide since 1850. *Scientific Data* **2023**, *10* (1), 155. DOI: 10.1038/s41597-023-02041-1.
(2) Lu, G.; Wang, Z.; Bhatti, U. H.; Fan, X. Recent progress in carbon dioxide capture technologies: A review. *Clean Energy Science and Technology* **2023**, *1* (1), 32. DOI: 10.18686/cest.v1i1.32 (acccessed 2024/12/17).
(3) Chowdhury, S.; Kumar, Y.; Shrivastava, S.; Patel, S. K.; Sangwai, J. S. A Review on the Recent Scientific and Commercial Progress on the Direct Air Capture Technology to Manage Atmospheric CO2 Concentrations and Future Perspectives. *Energy & Fuels* **2023**, *37* (15), 10733-10757. DOI: 10.1021/acs.energyfuels.2c03971.
(4) Livescu, A.; Navar, R.; Mangalindan, J. R.; Mahnaz, F.; Ge, Y.; Shetty, M.; Yang, X. Catalysts for Clean Energy: A Review on Current Progress for the Catalyzed Recycling of CO2 into Dimethyl Ether. *Topics in Catalysis* **2024**. DOI: 10.1007/s11244-024-01913-z.
(5) Otto, A.; Grube, T.; Schiebahn, S.; Stolten, D. Closing the loop: Captured CO2 as a feedstock in the chemical industry. *Energy and Environmental Science* **2015**, *8* (11), 3283-3297. DOI: 10.1039/c5ee02591e.
(6) Schmal, M.; Gonzalez Caranton, A. R.; Kozonoe, C. E.; Roseno, K. T. d. C.; Cavalcanti, F. M.; Brito Alves, R. M.; Giudici, R. Chapter 2 - Use of CO2 as a source for obtaining value-added products. In *Heterogeneous Catalysis*, Cesario, M. R., de Macedo, D. A. Eds.; Elsevier, 2022; pp 19-58.
(7) Hepburn, C.; Adlen, E.; Beddington, J.; Carter, E. A.; Fuss, S.; Mac Dowell, N.; Minx, J. C.; Smith, P.; Williams, C. K. The technological and economic prospects for CO2 utilization and removal. *Nature* **2019**, *575* (7781), 87-97. DOI: 10.1038/s41586-019-1681-6.
(8) Mahnaz, F.; Dunlap, V.; Helmer, R.; Borkar, S. S.; Navar, R.; Yang, X.; Shetty, M. Selective Valorization of CO2 towards Valuable Hydrocarbons through Methanol-mediated Tandem Catalysis. *ChemCatChem* **2023**, *15* (17), e202300402. DOI: https://doi.org/10.1002/cctc.202300402.
(9) Mahnaz, F.; Mangalindan, J. R.; Vito, J.; Helmer, R.; Shetty, M. Influence of acid strength on olefin selectivity of chabazite (CHA) framework zeolite/zeotype during tandem CO2 hydrogenation. *Journal of Catalysis* **2024**, *434*, 115518. DOI: https://doi.org/10.1016/j.jcat.2024.115518.
(10) Putrasari, Y.; Lim, O. Dimethyl Ether as the Next Generation Fuel to Control Nitrogen Oxides and Particulate Matter Emissions from Internal Combustion Engines: A Review. *ACS Omega* **2022**, *7*, 32-37. DOI: 10.1021/acsomega.1c03885.
(11) Catizzone, E.; Freda, C.; Braccio, G.; Frusteri, F.; Bonura, G. Dimethyl ether as circular hydrogen carrier: Catalytic aspects of hydrogenation/dehydrogenation steps. *Journal of Energy Chemistry* **2021**, *58*, 55-77. DOI: 10.1016/j.jechem.2020.09.040.
(12) Azizi, Z.; Rezaeimanesh, M.; Tohidian, T.; Rahimpour, M. R. Dimethyl ether: A review of technologies and production challenges. *Chemical Engineering and Processing: Process Intensification* **2014**, *82*, 150-172. DOI: 10.1016/j.cep.2014.06.007.
(13) Arya, P. K.; Tupkari, S.; Satish, K.; Thakre, G. D.; Shukla, B. M. DME blended LPG as a cooking fuel option for Indian household: A review. *Renewable and Sustainable Energy Reviews* **2016**, *53*, 1591-1601. DOI: 10.1016/j.rser.2015.09.007.
(14) Catizzone, E.; Bonura, G.; Migliori, M.; Frusteri, F.; Giordano, G. CO2 recycling to dimethyl ether: State-of-the-art and perspectives. *Molecules* **2018**, *23*. DOI: 10.3390/molecules23010031.
(15) Liu, C.; Liu, Z. Perspective on CO2 Hydrogenation for Dimethyl Ether Economy. *Catalysts* **2022**, *12*. DOI: 10.3390/catal12111375.
(16) Chen, X.; Su, T.; Luo, X.; Xie, X.; Qin, Z.; Ji, H. Catalytic hydrogenation of CO2 to DME on surface Cu via highly efficient electron redistribution at the Cu0/Cu+ interface. *Surfaces and Interfaces* **2024**, *48*, 104346. DOI: https://doi.org/10.1016/j.surfin.2024.104346.

(17) Mota, N.; Millán Ordoñez, E.; Pawelec, B.; Fierro, J. L. G.; Navarro, R. M. Direct Synthesis of Dimethyl Ether from CO2: Recent Advances in Bifunctional/Hybrid Catalytic Systems. *Catalysts* **2021**, *11* (4). DOI: 10.3390/catal11040411.
(18) Frusteri, F.; Migliori, M.; Cannilla, C.; Frusteri, L.; Catizzone, E.; Aloise, A.; Giordano, G.; Bonura, G. Direct CO2-to-DME hydrogenation reaction: New evidences of a superior behaviour of FER-based hybrid systems to obtain high DME yield. *Journal of CO2 Utilization* **2017**, *18*, 353-361. DOI: 10.1016/j.jcou.2017.01.030.
(19) Climent, M. J.; Corma, A.; Iborra, S.; Sabater, M. J. Heterogeneous Catalysis for Tandem Reactions. *ACS Catalysis* **2014**, *4* (3), 870-891. DOI: 10.1021/cs401052k.
(20) Gioria, E.; Duarte-Correa, L.; Bashiri, N.; Hetaba, W.; Schomaecker, R.; Thomas, A. Rational design of tandem catalysts using a core-shell structure approach. *Nanoscale Adv* **2021**, *3* (12), 3454-3459. DOI: 10.1039/d1na00310k From NLM.
(21) Álvarez, A.; Bansode, A.; Urakawa, A.; Bavykina, A. V.; Wezendonk, T. A.; Makkee, M.; Gascon, J.; Kapteijn, F. Challenges in the Greener Production of Formates/Formic Acid, Methanol, and DME by Heterogeneously Catalyzed CO2 Hydrogenation Processes. *Chemical Reviews* **2017**, *117*, 9804-9838. DOI: 10.1021/acs.chemrev.6b00816.
(22) Wang, W.; Zeng, C.; Tsubaki, N. Recent advancements and perspectives of the CO2 hydrogenation reaction. *Green Carbon* **2023**, *1* (2), 133-145. DOI: https://doi.org/10.1016/j.greenca.2023.10.003.
(23) Arena, F.; Italiano, G.; Barbera, K.; Bordiga, S.; Bonura, G.; Spadaro, L.; Frusteri, F. Solid-state interactions, adsorption sites and functionality of Cu-ZnO/ZrO2 catalysts in the CO2 hydrogenation to CH3OH. *Applied Catalysis A: General* **2008**, *350* (1), 16-23. DOI: 10.1016/j.apcata.2008.07.028.
(24) Arena, F.; Barbera, K.; Italiano, G.; Bonura, G.; Spadaro, L.; Frusteri, F. Synthesis, characterization and activity pattern of Cu–ZnO/ZrO2 catalysts in the hydrogenation of carbon dioxide to methanol. *Journal of Catalysis* **2007**, *249* (2), 185-194. DOI: https://doi.org/10.1016/j.jcat.2007.04.003.
(25) Li, C.; Yuan, X.; Fujimoto, K. Development of highly stable catalyst for methanol synthesis from carbon dioxide. *Applied Catalysis A: General* **2014**, *469*, 306-311. DOI: https://doi.org/10.1016/j.apcata.2013.10.010.
(26) Wang, Y. H.; Gao, W. G.; Wang, H.; Zheng, Y. E.; Na, W.; Li, K. Z. Structure–activity relationships of Cu–ZrO2 catalysts for CO2 hydrogenation to methanol: interaction effects and reaction mechanism. *RSC Advances* **2017**, *7* (14), 8709-8717, 10.1039/C6RA28305E. DOI: 10.1039/C6RA28305E.
(27) Raudaskoski, R.; Niemelä, M. V.; Keiski, R. L. The effect of ageing time on co-precipitated Cu/ZnO/ZrO 2 catalysts used in methanol synthesis from CO 2 and H 2. *Topics in Catalysis* **2007**, *45*, 57-60. DOI: 10.1007/s11244-007-0240-9.
(28) Li, L.; Mao, D.; Yu, J.; Guo, X. Highly selective hydrogenation of CO2 to methanol over CuO-ZnO-ZrO2 catalysts prepared by a surfactant-assisted co-precipitation method. *Journal of Power Sources* **2015**, *279*, 394-404. DOI: 10.1016/j.jpowsour.2014.12.142.
(29) Huang, C.; Chen, S.; Fei, X.; Liu, D.; Zhang, Y. Catalytic Hydrogenation of CO2 to Methanol: Study of Synergistic Effect on Adsorption Properties of CO2 and H2 in CuO/ZnO/ZrO2 System. *Catalysts* **2015**, *5* (4), 1846-1861. DOI: 10.3390/catal5041846.
(30) Witoon, T.; Kachaban, N.; Donphai, W.; Kidkhunthod, P.; Faungnawakij, K.; Chareonpanich, M.; Limtrakul, J. Tuning of catalytic CO2 hydrogenation by changing composition of CuO-ZnO-ZrO2 catalysts. *Energy Conversion and Management* **2016**, *118*, 21-31. DOI: 10.1016/j.enconman.2016.03.075.
(31) Bonura, G.; Cordaro, M.; Spadaro, L.; Cannilla, C.; Arena, F.; Frusteri, F. Hybrid Cu–ZnO–ZrO2/H-ZSM5 system for the direct synthesis of DME by CO2 hydrogenation. *Applied Catalysis B: Environmental* **2013**, *140-141*, 16-24. DOI: https://doi.org/10.1016/j.apcatb.2013.03.048.
(32) Wild, S.; Lacerda de Oliveira Campos, B.; Zevaco, T. A.; Guse, D.; Kind, M.; Pitter, S.; Herrera Delgado, K.; Sauer, J. Experimental investigations and model-based optimization of CZZ/H-FER 20 bed compositions for the direct synthesis of DME from CO2-rich syngas. *Reaction Chemistry and Engineering* **2022**, *7* (4), 943-956. DOI: 10.1039/d1re00470k.

(33) Frusteri, F.; Cordaro, M.; Cannilla, C.; Bonura, G. Multifunctionality of Cu-ZnO-ZrO2/H-ZSM5 catalysts for the one-step CO2-to-DME hydrogenation reaction. *Applied Catalysis B: Environmental* **2015**, *162*, 57-65. DOI: 10.1016/j.apcatb.2014.06.035.
(34) Zhou, X.; Su, T.; Jiang, Y.; Qin, Z.; Ji, H.; Guo, Z. CuO-Fe2O3-CeO2/HZSM-5 bifunctional catalyst hydrogenated CO2 for enhanced dimethyl ether synthesis. *Chemical Engineering Science* **2016**, *153*, 10-20. DOI: 10.1016/j.ces.2016.07.007.
(35) Pop, G.; Bozga, G.; Ganea, R.; Natu, N. Methanol conversion to dimethyl ether over H-SAPO-34 catalyst. *Industrial and Engineering Chemistry Research* **2009**, *48* (15), 7065-7071. DOI: 10.1021/ie900532y.
(36) Pop, G.; Theodorescu, C. SAPO-34 catalyst for dimethylether production. *Studies in Surface Science and Catalysis* **2000**, *130*, 287-292. DOI: https://doi.org/10.1016/S0167-2991(00)80971-4.
(37) Natesakhawat, S.; Lekse, J. W.; Baltrus, J. P.; Ohodnicki, P. R., Jr.; Howard, B. H.; Deng, X.; Matranga, C. Active Sites and Structure–Activity Relationships of Copper-Based Catalysts for Carbon Dioxide Hydrogenation to Methanol. *ACS Catalysis* **2012**, *2* (8), 1667-1676. DOI: 10.1021/cs300008g.
(38) Pacchioni, G. From CO2 to Methanol on Cu/ZnO/Al2O3 Industrial Catalyst. What Do We Know about the Active Phase and the Reaction Mechanism? *ACS Catalysis* **2024**, *14* (4), 2730-2745. DOI: 10.1021/acscatal.3c05669.
(39) Li, K.; Chen, J. G. CO2 Hydrogenation to Methanol over ZrO2-Containing Catalysts: Insights into ZrO2 Induced Synergy. *ACS Catalysis* **2019**, *9* (9), 7840-7861. DOI: 10.1021/acscatal.9b01943.
(40) Stangeland, K.; Li, H.; Yu, Z. Thermodynamic Analysis of Chemical and Phase Equilibria in CO2 Hydrogenation to Methanol, Dimethyl Ether, and Higher Alcohols. *Industrial and Engineering Chemistry Research* **2018**, *57* (11), 4081-4094. DOI: 10.1021/acs.iecr.7b04866.
(41) Mahnaz, F.; Dharmalingam, B. C.; Mangalindan, J. R.; Vito, J.; Varghese, J. J.; Shetty, M. Metal cation exchange with zeolitic acid sites modulates hydrocarbon pool propagation during CO2 hydrogenation. *Chem Catalysis* **2024**, 101183. DOI: https://doi.org/10.1016/j.checat.2024.101183.
(42) Mahnaz, F.; Mangalindan, J. R.; Dharmalingam, B. C.; Vito, J.; Lin, Y. T.; Akbulut, M.; Varghese, J. J.; Shetty, M. Intermediate Transfer Rates and Solid-State Ion Exchange are Key Factors Determining the Bifunctionality of In2O3/HZSM-5 Tandem CO2 Hydrogenation Catalyst. *ACS Sustainable Chemistry and Engineering* **2024**, *12* (13), 5197-5210. DOI: 10.1021/acssuschemeng.3c08250.
(43) Wang, X.; Jeong, S. Y.; Jung, H. S.; Shen, D.; Ali, M.; Zafar, F.; Chung, C. H.; Bae, J. W. Catalytic activity for direct CO2 hydrogenation to dimethyl ether with different proximity of bifunctional Cu-ZnO-Al2O3 and ferrierite. *Applied Catalysis B: Environmental* **2023**, *327*. DOI: 10.1016/j.apcatb.2023.122456.
(44) Ateka, A.; Pérez-Uriarte, P.; Gamero, M.; Ereña, J.; Aguayo, A. T.; Bilbao, J. A comparative thermodynamic study on the CO2 conversion in the synthesis of methanol and of DME. *Energy* **2017**, *120*, 796-804. DOI: 10.1016/j.energy.2016.11.129.
(45) Peters, M. S.; Timmerhaus, K. D.; West, R. E. *Plant Design and Economics for Chemical Engineers*; McGraw-Hill Professional, 2002.
(46) Center for Sustainable Systems, U. o. M. *"Hydrogen Factsheet."*; 2024. https://css.umich.edu/publications/factsheets/energy/hydrogen-factsheet.
(47) IEA. *Global Hydrogen Review 2023*; IEA, Paris, 2023. https://www.iea.org/reports/global-hydrogen-review-2023.
(48) Congressional Budget Office. *Carbon Capture and Storage in the United States*; 2023. www.cbo.gov/publication/59345.
(49) IEA. *CCUS in clean energy transitions*; IEA, Paris, 2020. https://www.iea.org/reports/ccus-in-clean-energy-transitions.
(50) EIA. *How much carbon dioxide is produced per kilowatthour of U.S. electricity generation?* 2023. https://www.eia.gov/tools/faqs/faq.php?id=74&t=11 (accessed 2024 November 6).
(51) Chen, H.; Cui, H.; Lv, Y.; Liu, P.; Hao, F.; Xiong, W.; Luo, H. a. CO2 hydrogenation to methanol over Cu/ZnO/ZrO2 catalysts: Effects of ZnO morphology and oxygen vacancy. *Fuel* **2022**, *314*, 123035. DOI: https://doi.org/10.1016/j.fuel.2021.123035.

(52) Kattel, S.; Ramírez, P. J.; Chen, J. G.; Rodriguez, J. A.; Liu, P. Active sites for CO(2) hydrogenation to methanol on Cu/ZnO catalysts. *Science* **2017**, *355* (6331), 1296-1299. DOI: 10.1126/science.aal3573 From NLM.
(53) Behrens, M.; Studt, F.; Kasatkin, I.; Kühl, S.; Hävecker, M.; Abild-Pedersen, F.; Zander, S.; Girgsdies, F.; Kurr, P.; Kniep, B. L.; et al. The active site of methanol synthesis over Cu/ZnO/Al2O3 industrial catalysts. *Science* **2012**, *336* (6083), 893-897. DOI: 10.1126/science.1219831 From NLM.
(54) Palomino, R. M.; Ramírez, P. J.; Liu, Z.; Hamlyn, R.; Waluyo, I.; Mahapatra, M.; Orozco, I.; Hunt, A.; Simonovis, J. P.; Senanayake, S. D.; et al. Hydrogenation of CO2 on ZnO/Cu(100) and ZnO/Cu(111) Catalysts: Role of Copper Structure and Metal–Oxide Interface in Methanol Synthesis. *The Journal of Physical Chemistry B* **2018**, *122* (2), 794-800. DOI: 10.1021/acs.jpcb.7b06901.
(55) Amenomiya, Y. Methanol synthesis from CO2 + H2 II. Copper-based binary and ternary catalysts. *Applied Catalysis* **1987**, *30* (1), 57-68. DOI: https://doi.org/10.1016/S0166-9834(00)81011-8.
(56) Ledakowicz, S.; Nowicki, L.; Petera, J.; Niziol, J.; Kowalik, P.; Gołębiowski, A. Kinetic characterisation of catalysts for methanol synthesis. *Chemical and Process Engineering* **2013**, *34*. DOI: 10.2478/cpe-2013-0040.
(57) Beck, A.; Newton, M. A.; van de Water, L. G. A.; van Bokhoven, J. A. The Enigma of Methanol Synthesis by Cu/ZnO/Al2O3-Based Catalysts. *Chemical Reviews* **2024**, *124* (8), 4543-4678. DOI: 10.1021/acs.chemrev.3c00148.
(58) Detz, R. J.; Reek, J. N. H.; van der Zwaan, B. C. C. The future of solar fuels: when could they become competitive? *Energy & Environmental Science* **2018**, *11* (7), 1653-1669, 10.1039/C8EE00111A. DOI: 10.1039/C8EE00111A.

GRAPHICAL ABSTRACT